Input coupling systems for millimetre-wave gyrotron traveling wave amplifiers

Liang Zhang, Craig R. Donaldson, Jason Garner, Adrian W. Cross, and Wenlong He

Department of Physics, SUPA, University of Strathclyde, Glasgow, Scotland, G4 0NG, UK
*liang.zhang@strath.ac.uk

Abstract: Input couplers for mm-wave gyrotron traveling wave amplifiers are presented in this paper. A W-band input coupling system composed of a pillbox window, a smoothly curved waveguide bend, a T-junction and a broadband reflector was numerically optimized, constructed and measured. An average transmission coefficient of -2.0 dB over a designed operating frequency range was measured. Additionally a higher frequency input coupler for operation at a central frequency of 372 GHz was also designed based on a multiple-hole coupling configuration. The simulated transmission coefficient was -0.5 dB if Ohmic loss is not considered.

1. Introduction

Gyro-devices are coherent microwave radiation sources based on the cyclotron resonance maser instability [1]. They have superior power capability compared with slow-wave devices and are promising sources operating at millimetre and sub-millimetre wavelengths. Gyrotron traveling wave amplifiers (gyro-TWAs) can be used in applications such as telecommunication, RADAR, plasma diagnostics, electron paramagnetic resonance spectroscopy and so on, due to its high power and broadband capabilities.

Different interaction circuits have been successfully used in gyro-TWAs, including dielectric-loaded waveguides [2, 3] which have very high gain, photonic band gap circuits [4, 5] which have the advantage of operating with a higher order mode, and the helically corrugated interaction regions (HCIR) [6, 7] which are able to achieve wider bandwidth.

The HCIR was previously used in gyrotron backward wave oscillators [8], gyro-TWAs [6, 7] and microwave pulse compressors [9, 10] and have demonstrated excellent results. In a three-fold HCIR, the operating eigenwave is a result of coupling between the TE_{21} mode and the first spatial harmonic of the TE_{11} mode. By carefully choosing the dimensions of the HCIR, a constant group velocity of the wave can be achieved and matched to the velocity of an electron beam over a wide frequency range for efficient beam-wave interaction. Gyro-TWAs operating at mm-wavelengths are under development. A gyro-TWA at W-band has been designed, constructed and experimentally measured. In simulation, a ~40 dB gain and ~10% bandwidth can be achieved. While in the experiment, due to the limitation of the driving solid-state source, a maximum power of 3.4 kW in the driving frequency band of 91-96.5 GHz was measured [11]. Another amplifier was designed to operate with the same mode, but at a much higher centre frequency of 372 GHz. In simulations ~500 W output power over a bandwidth of 5% was predicted.

A schematic drawing of the gyro-TWAs is shown in Fig. 1. It includes the electron gun (1), magnetic coils (2, 3), input coupling system (4-7), elliptical polarizer (8), HCIR (9), output taper (10) and an output launcher with microwave window (11, 12) [12-14]. A diode with an annular electron emitter was used to form the electron beam which then propagated through a magnetic field cusp produced by the two magnetic coils initiating cyclotron motion around the longitudinal axis of the system [15]. The magnetic system served to confine and transport the electron beam, as well as to provide the required magnetic field strength in the interaction region. The input coupling system enabled the low power millimetre-wave signal, generated by a solid-state source, to couple into the interaction region.

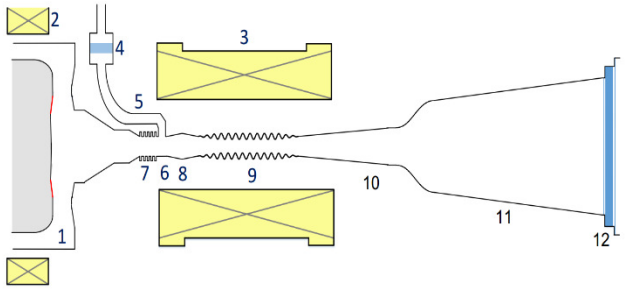

Fig. 1 The schematic of a gyro-TWA. (1) electron gun, (2, 3) magnetic coil system, (4) microwave window, (5) waveguide bend, (6) input mode converter, (7) broadband reflector, (8) elliptical polarizer, (9) HCIR, (10) waveguide taper, (11) output launcher, (12) output window.

The input coupling system not only separated the atmosphere from the ultra-high vacuum inside the gyro-TWA, but also ensured efficient mode coupling between the input modes from the TE_{10} mode in rectangular waveguide to the TE_{11} mode in the circular waveguide. If the losses or reflection from the input coupling system is too high then there a drop in the output power from the gyro-TWA requiring a higher power from the solid-state input source, which is costly. Undesired oscillations may also occur if the reflection sufficiently large.

The input systems for both amplifiers was briefly introduced in [16]. In this paper, more detail description on the simulation and measurement results of the input couplers operating at W-band are presented, while at higher frequency the simulation results will be presented alongside discussion on the challenge of manufacturing the optimized coupler.

2. Design and measurement of the W-band input coupling system

The whole input coupling system consisted of a microwave window, a waveguide bend and a mode convertor, which are labelled (4), (5) and (6) in Fig. 1. To achieve the

optimal transmission, every component needs to be carefully designed and optimized.

The microwave window was chose to be the pillbox type [17]. It had the advantage of achieving a balanced performance between bandwidth and transmission; it can also directly connect to the solid-state source. The initial dimensions of the pillbox window were evaluated from analytical equations and further optimized through the mode-matching method. An impedance matching section was added between the rectangular waveguide and the circular cavity to further improve the bandwidth performance. The optimized geometry was verified by CST microwave studio [18]. The pillbox window was designed to be demountable from the input coupler in order that it could be changed or reused. On one side a custom-sized stainless flange with CF-like knife edge was vacuum brazed onto the rectangular waveguide, while on the other end was a standard WR-10 UG-387/U round flange. Fig. 2 shows the 3D drawing of the pillbox window, and Fig. 3 is its practical assembly, alongside the measured millimetre-wave transmission.

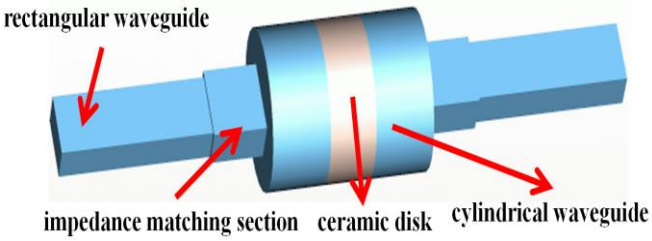

Fig. 2 3D model of the designed pillbox window

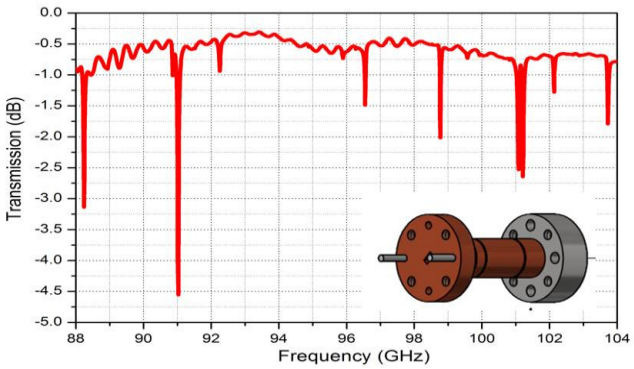

Fig. 3 the measured transmission through the pillbox with assembly drawing inset.

In the input coupling system, a 90° waveguide bend was required due to physical constrains of the gyro-TWA. The mitre and smoothly curved type bends were investigated. In theory, both kinds should be able to achieve negligible reflection if properly designed. However a tolerance study showed that the mitre bend was sensitive to the mitre angle. Also, the machining of the mitre bend would be more difficult than the smoothly curved bend. Therefore the final waveguide bend was chosen to be a smoothly curved one. Fig. 4 shows one smoothly curved waveguide bend made for test. The reflection was measured to be better than -30 dB and the transmission loss is 0.6 dB on average in the chosen frequency band.

A prototype of an input mode convertor for the W-band gyro-TWA has been studied and measured [19]. The mode conversion between the TE_{10} mode in rectangular waveguide and the TE_{11} mode in circular waveguide was achieved by a T-junction. It was chosen because there is limited space between the water cooled solenoid system and the beam tube. The T-junction has the simplest structure and minimum brazing area. To enhance the mode conversion efficiency as well as increase the bandwidth, a broadband reflector was placed at the electron gun side to stop the input microwave signal propagating to the electron gun region. The inner diameter of the reflector was chosen large enough to reduce the possibility of the beam interception. The prototype of the input coupler achieved an average transmission of -1.0 dB over the frequency range of 90 - 100 GHz.

Fig. 4 A photo of a smoothly curved waveguide bend made for test.

After verifying the concept, an input coupling system was machined and integrated into the W-band gyro-TWA system. The T-junction was directly machined on the beam tube, which supports all the waveguide components, including the elliptical polarizer, HCIR and waveguide taper to connect the HCIR and output launcher. The waveguide bend, vacuum flange, and beam tube were then brazed together and vacuum leak tested to holding a vacuum of better than 1E-9 mbar when pumped by an ion pump.

The millimetre-wave property of the manufactured input coupling system was then measured by an Anritsu vector network analyser (VNA, model ME7808). The measurement setup is shown in Fig. 5 with all the individual components, including elliptical polarizers, HCIR, waveguide tapers inserted within the stainless steel tube. This allowed the millimetre-wave properties including Ohmic loss to be calibrated for each component. During the measurement, the position of the broadband reflector was finely adjusted in order to achieve the highest transmission coefficient.

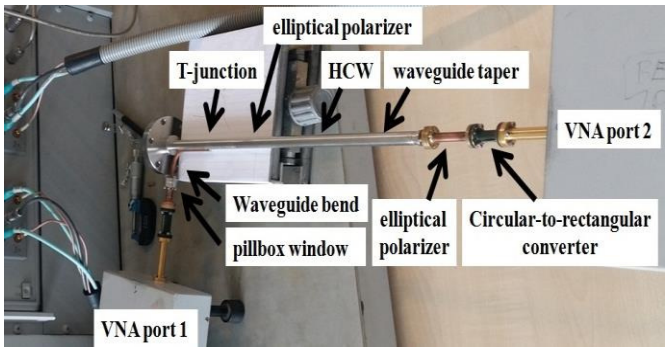

Fig. 5 VNA measurement setup of the W-band input coupling system.

Table 1 Ohmic loss of individual component

Component	Loss (dB)
pillbox window	0.6
waveguide bend	0.4
elliptical polarizers 1	0.9
HCW	1.5
waveguide taper	1.0
elliptical polarizers 2	0.6
circular-to-rectangular converter	0.3

A summary of the average loss from each component over the interested frequency range is listed in Table 1. The loss of the input coupling system can therefore be obtained. The transmission coefficient of the whole measured circuit is better than -6 dB over the interested frequency of 90 – 100 GHz, as shown in Fig. 6. The loss of the whole input coupling system is about -2.0 dB, which includes the loss from the pillbox window and the waveguide bends, but exclude the loss of the helically corrugated waveguide and the elliptical polarizers.

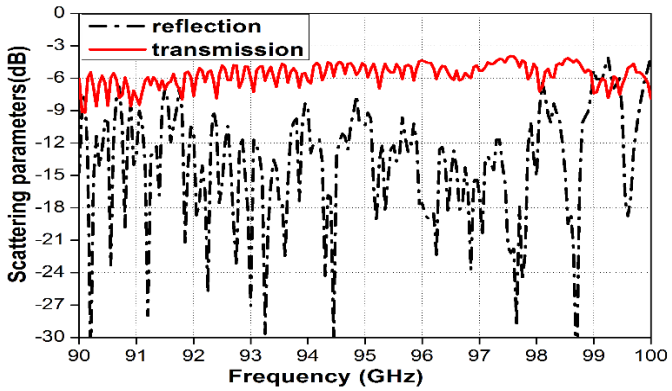

Fig. 6 The measurement setup of the input coupler system at W-band.

3. Input coupler for high frequency gyro-amplifier

Another gyro-TWA operating at a higher centre frequency of 372 GHz is being designed. As the frequency becomes higher the waveguide component geometrical dimensions become smaller. This gives rise to two major challenges in the realization of an input coupler, i.e., increased sensitivity to machining tolerance and higher transmission loss. The millimetre-wave properties of the high frequency input coupling system would be very sensitive to the manufacturing tolerance as the dimensions of the rectangular waveguide in this case would be approximately 0.5 mm × 0.33 mm. Also the period of the broadband reflector would be less than 0.2 mm, which would be very challenging to manufacture.

To decrease the machining difficulty, a small-aperture multiple-hole input coupler was considered [20, 21]. The coupling coefficient of a single hole can be derived from the small aperture theory [22]. The coupled microwave power can be enhanced or cancel out each other by adjusting the distance of multiple holes.

The aperture size would be small at high frequency, however after examining different aperture shapes, such as circular and rectangular holes, in CST microwave studio simulation, it was found that the aperture shape itself does not significantly affect the coupling coefficient. Both circular and rectangular apertures could achieve the desired performance. This feature is helpful because laser machining could therefore be used to create these small circular apertures.

A multiple-hole coupler is a 4-port waveguide component, as shown in Fig. 7. By carefully choosing the distance between the apertures as-well-as their aperture sizes high coupling coefficient between the desired modes, i.e., TE_{10} and TE_{11}, could be achieved. The multiple-hole coupler also has the advantage of a high directivity which would help to stop the microwave signal traveling back to the electron gun region.

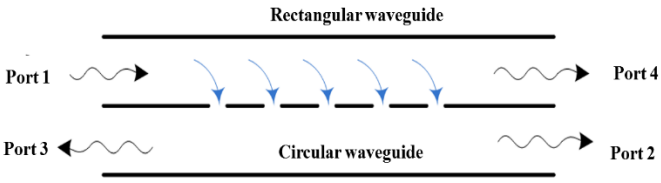

Fig. 7 Power flow of the 4-port directional coupler.

The performance, such as the bandwidth and the directivity, could be improved by increasing the number of the holes. However the Ohmic loss would also increase due to the increase in the structure length. An optimized multiple-coupler operating at a central frequency of 372 GHz contained 12 identical holes, as shown in Fig. 8. The separation distance between the circular and rectangular waveguide should be as small as possible to reduce the power loss. In the simulation, a value of 0.05 mm was chosen. In the simulation, it was able to achieve a transmission coefficient better than -0.5 dB without considering the Ohmic loss. Due to the short structure length the transmission loss was approximately 0.4 dB, as shown in Fig 9, when the conductivity of the material was set to be one tenth of pure copper.

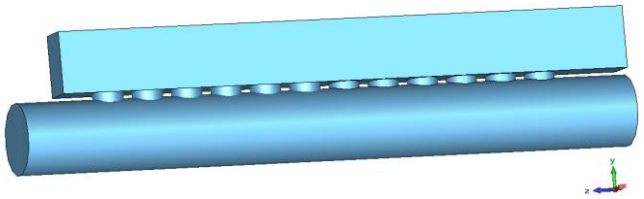

Fig. 8 The CST model of the multiple-hole coupler.

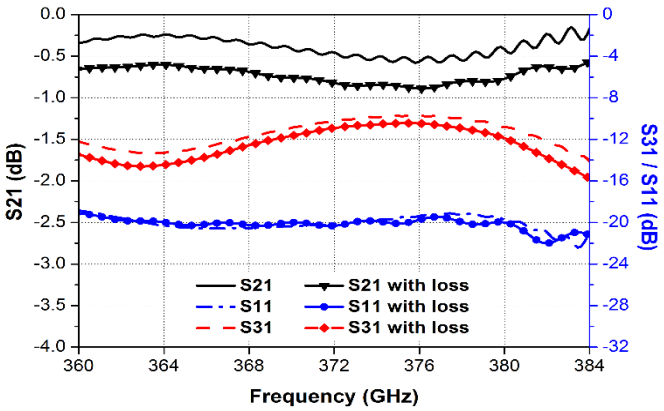

Fig. 9 The simulation results of the multiple-hole coupler.

Fig. 10 shows the CAD drawing and assembly of the multiple-hole coupler. The structure was divided into 3 parts for ease of fabrication. Parts 1 and 2 were relatively simple structures and could be made through the wire-cutting technique. Part 3, including the frame and the circular waveguide, could also be machined by a wire-cutting technique, and the aperture holes could be made through laser machining or micro drilling. The three parts are currently being machined. These parts will be assembled together to form a complete multiple-hole coupler and will be experimentally measured using a VNA.

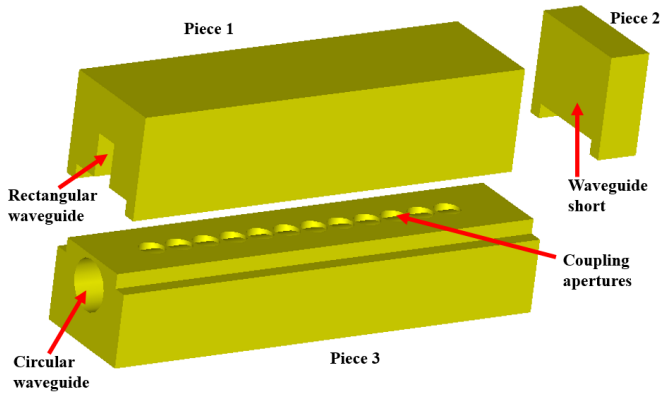

Fig. 10 3D drawing and assembly of the multiple-hole coupler.

4. Conclusion

In this paper, two input couplers, operating at W-band and Y-band, were designed. The W-band input coupler has been successfully manufactured and used in the W-band gyro-TWA experiments achieving excellent results. The higher frequency input coupler for operation at a centre frequency of 372-GHz is currently being manufactured and its performance will be measured and reported in the future.

5. Acknowledgments

This work was supported by the Engineering and Physical Sciences Research Council (EPSRC) U.K. under Research Grant EP/K029746/1, and Science and Technology Facilities Council (STFC) under Research Grant ST/P001890/1.

6. References

[1] Chu, K.R.: 'The electron cyclotron maser,' Rev. Modern Phys., 2004, 76, (2), pp. 489–540.

[2] Yan, R., Tang, Y. Luo, Y.: 'Design and experimental study of a high-gain W-band gyro-TWT with nonuniform periodic dielectric loaded waveguide,' IEEE Trans. Electron Devices, 2014, 61, (7), pp. 2564–2569.

[3] Song, H. H., McDermott, D. B., Hirata, Y., et al.: 'Theory and experiment of a 94 GHz gyrotron traveling-wave amplifier,' Physics of Plasmas, 2004,11, (5), pp. 2935-2941.

[4] Nanni, E.A., Lewis, S.M., Shapiro, M.A., et al.: 'Photonic-band-gap traveling-wave gyrotron amplifier,' Phys. Rev. Lett., 2013, 111, (23), pp. 235101-1–235101-5.

[5] Kim, H. J. , Nanni, E. A., Shapiro, M. A. et al.: 'Amplification of picosecond pulses in a 140-GHz gyrotron-traveling wave tube,' Phys. Rev. Lett., 2010, 105, (13), p. 135101.

[6] Bratman, V. L., Cross, A. W., Denisov, G. G., et al.: 'High-gain wide-band gyrotron traveling wave amplifier with a helically corrugated waveguide,' Phys. Rev. Lett., 2000, 84, (12), pp. 2746-2749.

[7] Cross, A. W., He, W., Phelps, A. D. R., et al.: 'Helically corrugated waveguide gyrotron traveling wave amplifier using a thermionic cathode electron gun,' Appl. Phys. Lett., 2007, 90, (25), p. 253501.

[8] He, W., Donaldson, C. R., Zhang, L., et al.: 'High power wideband gyrotron backward wave oscillator operating towards the terahertz region,' Phys. Rev. Lett., 2013, 110, (16), p. 165101.

[9] Samsonov, S. V., Phelps, A. D. R., Bratman, V. L., et al.:'Compression of Frequency-Modulated Pulses using Helically Corrugated Waveguides and Its Potential for Generating Multigigawatt RF Radiation,' Phys. Rev. Lett., 2004, 92, (11), pp. 118301.

[10] Zhang, L., Mishakin, S.V., He, W., et al.: 'Experimental Study of Microwave Pulse Compression Using a Five-Fold Helically Corrugated Waveguide,' in IEEE Transactions on Microwave Theory and Techniques, 2015, 63, (3), pp. 1090-1096.

[11] He, W., Donaldson, C. R., Zhang, L., et al.: 'Broadband amplification of low-terahertz signals using axis-encircling electrons in a helically corrugated interaction region,' Phys. Rev. Lett., 2017, 119, (18), p. 184801.

[12] Zhang, L., He, W., Donaldson, C.R., et al.: 'Optimization and Measurement of a Smoothly Profiled Horn for a W-Band Gyro-TWA,' IEEE Trans. Electron Devices, 2017, 64, (6), pp. 2665-2669.

[13] McElhinney, P., Donaldson, C.R., McKay, J. E., et al.: 'An output coupler for a W-band high power wideband gyro-amplifier,' IEEE Trans. Electron Devices, 2017, 64, (4), pp. 1763-1766.

[14] Donaldson, C. R., McElhinney, P., Zhang, L., et al.: 'Wide-band HE_{11} mode terahertz wave windows for gyro-amplifiers,' IEEE Trans. THz Sci. Technol., 2016, 6, (1), pp. 108-112.

[15] Donaldson, C.R., He, W., Cross, A. W., et al.: 'A cusp electron gun for millimeter wave gyrodevices,' Appl. Phys. Lett., 2010, 96, (14), p. 141501.

[16] Zhang, L., Donaldson, C.R., Garner, J.R., et al.: 'Input coupling systems for mm-wave amplifiers,' 2017, 10th UK-Europe-China Workshop on Millimetre Waves and Terahertz Technologies (UCMMT), Sept. 2017, pp. 1-2.

[17] Zhu, F., Zhang, Z.C., Luo J. R., et al.: 'Investigation of the Failure Mechanism for an S-Band Pillbox Output Window Applied in High-Average-Power Klystrons," IEEE Trans. Electron Devices, 2010, 57, (4), pp. 946-951.

[18] CST Corp. CST MWS Tutorials, accessed on Dec. 1, 2016. [Online].

[19] Zhang, L., He, W., Donaldson, C.R., et al.: 'Design and measurement of a broadband sidewall coupler for a W-band gyro-TWA,' IEEE Trans. Microw. Theory Techn., 2015, 63, (10), pp. 3183-3190.

[20] Garner, J.R., Zhang, L., Donaldson, C.R., et al.: 'Design Study of a Fundamental Mode Input Coupler for a 372-GHz Gyro-TWA I: Rectangular-to-Circular Coupling Methods,' IEEE Trans. Electron Devices, 2016, 63, (1), pp. 497-503.

[21] Garner, J.R., Zhang, L., Donaldson, C.R., et al.: 'Design Study of a 372-GHz Higher Order Mode Input Coupler,' IEEE Trans. Electron Devices, 2016, 63, (8), pp. 3284-3289.

[22] Pozar, D. M.: 'Microwave Engineering,' chapter 4, 4th Edition, John Wiley & Sons, Inc., 2011.